

RESTRICTED N 62 59837

Copy No. 311

RM No. L8I03

NACA RM No. L8I03



RESEARCH MEMORANDUM

CLASSIFICATION CHANGED TO
UNCLASSIFIED
AUTHORITY CROWLEY CHANGE #2007
DATE 12-14-53 T.C.F.

THE EFFECTS OF HIGH-LIFT DEVICES ON THE LOW-SPEED STABILITY
CHARACTERISTICS OF A TAPERED 37.5° SWEPTBACK WING OF
ASPECT RATIO 3 IN STRAIGHT AND ROLLING FLOW

By

M. J. Queijo and Jacob H. Lichtenstein

Langley Aeronautical Laboratory
Langley Field, Va.

CLASSIFIED DOCUMENT

This document contains classified information affecting the National Defense of the United States within the meaning of the Espionage Act, USC 50:31 and 32. Its transmission or the revelation of its contents in any manner to an unauthorized person is prohibited by law. Information so classified may be imparted only to persons in the military and naval services of the United States, appropriate civilian officers and employees of the Federal Government who have a legitimate interest therein, and to United States citizens of known loyalty and discretion who of necessity must be informed thereof.

NATIONAL ADVISORY COMMITTEE FOR AERONAUTICS

WASHINGTON

November 9, 1948

RESTRICTED

NATIONAL ADVISORY COMMITTEE FOR AERONAUTICS

RESEARCH MEMORANDUM

THE EFFECTS OF HIGH-LIFT DEVICES ON THE LOW-SPEED STABILITY
CHARACTERISTICS OF A TAPERED 37.5° SWEEPBACK WING OF
ASPECT RATIO 3 IN STRAIGHT AND ROLLING FLOW

By M. J. Queijo and Jacob H. Lichtenstein

SUMMARY

An investigation has been conducted in the 6-foot circular test section of the Langley stability tunnel to determine the effects of split flaps, nose flaps, and slats in various combinations on the stability characteristics in straight and rolling flow of a 37.5° sweptback wing of aspect ratio 3, taper ratio 0.49, and NACA 23012 airfoil sections normal to the wing trailing edge. The Mach number and Reynolds number of the tests were 0.13 and 1,020,000, respectively.

The results of the investigation indicate that the variation of the parameters with lift coefficient is essentially the same at low and moderate lift coefficients for all the configurations tested. The high-lift devices extended the initial trend of the derivatives to higher lift coefficients, and in some cases also caused small displacements of the curves plotted against lift coefficient. Nose flaps were not as effective as slats in extending the initial trend of the curves to high lift coefficients. Combinations of split flaps and slats produced effects which were approximately equal to the sum of the effects of split flaps alone and slats alone.

INTRODUCTION

Estimation of the dynamic flight characteristics of aircraft requires a knowledge of the component forces and moments resulting from the orientation of the airplane with respect to the air stream and from the angular velocity of the airplane about each of its three axes. The forces and moments resulting from the orientation of the airplane normally are expressed as the static stability derivatives which are readily determined in conventional wind-tunnel tests. The forces and moments related to the angular motions generally are expressed as the rotary derivatives and usually have been estimated from theory because of the lack of a convenient experimental technique.

In the Langley stability tunnel both the rotary and static stability derivatives can be determined with about the same ease, and a comprehensive program is now under way to determine the effects of various geometric variables on both the rotary and static stability characteristics of wings and complete airplane configurations. A previous investigation into the effect of high-lift devices in yawing flow was reported in reference 1. The present investigation is concerned with the determination of the influence of various high-lift devices on the static and rolling characteristics of a 37.5° sweptback wing of aspect ratio 3, taper ratio 0.49, and NACA 23012 airfoil sections normal to the wing trailing edge. The wing was tested in combination with a circular fuselage.

SYMBOLS

The results of the tests are presented as standard NACA coefficients of forces and moments which are referred to the system of stability axes (fig. 1) with the origin at the projection on the plane of symmetry of the quarter-chord point of the mean aerodynamic chord of the model (fig. 2). The symbols and coefficients used herein are defined as follows:

C_L	lift coefficient	$\left(\frac{L}{qS}\right)$
C_X	longitudinal-force coefficient	$\left(\frac{X}{qS}\right)$
C_Y	lateral-force coefficient	$\left(\frac{Y}{qS}\right)$
C_l	rolling-moment coefficient	$\left(\frac{L'}{qSb}\right)$
C_n	yawing-moment coefficient	$\left(\frac{N}{qSb}\right)$
C_m	pitching-moment coefficient	$\left(\frac{M}{qS\bar{c}}\right)$
L	lift, pounds	
X	longitudinal force, pounds	
Y	lateral force, pounds	
L'	rolling moment, foot-pounds	
N	yawing moment, foot-pounds	

M	pitching moment, foot-pounds
q	dynamic pressure, pounds per square foot $\left(\frac{\rho V^2}{2}\right)$
ρ	mass density of air, slugs per cubic foot
V	free-stream velocity, feet per second
S	wing area, square feet (3.93 sq ft)
b	wing span, feet (3.24 ft)
c	chord of wing, measured parallel to plane of symmetry, feet
\bar{c}	mean aerodynamic chord, feet (1.096 ft) $\left(\frac{2}{S} \int_0^{b/2} c^2 dy\right)$
c'	local wing chord measured perpendicular to the wing quarter-chord line, feet
x	longitudinal distance from the root-chord leading edge to the quarter chord at any spanwise station, feet
\bar{x}	longitudinal distance from the root-chord leading edge to the aerodynamic center, feet (0.904 ft)
y	perpendicular distance from the root chord to any point on the quarter-chord line, feet
A	aspect ratio $\left(\frac{b^2}{S}\right)$
Λ	angle of sweep, positive for sweepback, degrees (37.5°)
λ	taper ratio, ratio of tip chord to root chord (0.49)
ψ	angle of yaw, degrees
α	angle of attack, degrees
p	rate of roll, radians per second
$\frac{pb}{2V}$	wing-tip helix angle, radians

$$C_{L\alpha} = \frac{\partial C_L}{\partial \alpha}$$

$$C_{Y\psi} = \frac{\partial C_Y}{\partial \psi}$$

$$C_{n\psi} = \frac{\partial C_n}{\partial \psi}$$

$$C_{l\psi} = \frac{\partial C_l}{\partial \psi}$$

$$C_{Y_p} = \frac{\partial C_Y}{\frac{\alpha_{pb}}{2V}}$$

$$C_{n_p} = \frac{\partial C_n}{\frac{\alpha_{pb}}{2V}}$$

$$C_{l_p} = \frac{\partial C_l}{\frac{\alpha_{pb}}{2V}}$$

MODEL AND APPARATUS

The tests of the present investigation were made in the 6-foot circular test section of the Langley stability tunnel. This section is equipped with a motor-driven rotor which imparts a twist to the air stream so that a model mounted rigidly in the tunnel is in a field of flow similar to that which exists about an airplane in rolling flight (reference 2).

The wing used in this investigation was made of mahogany and had 37.5° sweepback of the quarter-chord line, aspect ratio 3, taper ratio 0.49, and NACA 23012 airfoil sections in planes normal to the wing trailing edge. The wing was mounted in a circular fuselage so that its root chord coincided with the fuselage center line. Figure 2 is a drawing of the basic model of this investigation.

The high-lift devices used with the wing-fuselage combination were slats, nose flaps, and split flaps (fig. 3). All slats had chords which were 10 percent of the wing chord (measured normal to the wing quarter-chord line) and all split flaps had chords which were 20 percent of the wing chord (normal to wing quarter-chord line). The slats were made by

bending strips of $\frac{1}{16}$ -inch aluminum sheet to fit the contour of the wing leading edge. A $\frac{1}{8}$ -inch-wide strip of aluminum was riveted to the lower surface of the slat leading edge, and then the leading edge was rounded smooth. This simplified construction probably did not result in ideal slat contours, but it should be adequate for providing qualitative indications of the effects of slats on the parameters investigated.

The nose flaps were simulated by placing the slat trailing edge against the wing leading edge. Some overlap of the nose flap over the wing leading edge was necessary for proper mounting and, therefore, the nose-flap chord was about 9 percent of the wing chord.

A deflection of 60° was used for all the split flaps. Nose flaps and slats were deflected 50° .

Tests were made of the 10 model configurations indicated in figure 4. The word "wing" is applied to the wing-fuselage combination. The slats referred to as 0.5-span slats extended from the $0.5\frac{b}{2}$ station to the wing tip, and the split flap referred to as the 0.5-span split flaps extended from the wing-fuselage juncture to the $0.5\frac{b}{2}$ station.

The model was mounted on a single-strut support into which was built a six-component strain-gage balance system by which all the forces and moments on the model could be measured. Figure 5 is a photograph of one of the model configurations in the rolling-flow test section of the Langley stability tunnel.

TESTS

Two series of tests were made. The first series consisted of straight-flow tests in which the model yaw angle was varied from -5° to 5° , and the angle of attack was varied from about -4° up to or slightly beyond the stall angle. The second series of tests was made in rolling flow and covered the same angle-of-attack range as that used in straight flow. The rolling-flow tests were made at zero angle of yaw and simulated rates of roll corresponding to values of $pb/2V$ of 0, ± 0.0268 , and ± 0.0802 .

All tests were made at a dynamic pressure of 24.9 pounds per square foot, which corresponds to a Mach number of 0.13 and a Reynolds number of 1,020,000 based on the model mean aerodynamic chord (1.096 ft).

CORRECTIONS

Approximate corrections, based on unswept-wing theory, for the effects of the jet boundaries have been applied to the angle of attack and the longitudinal-force coefficient. No tare corrections were applied to the data nor were the data corrected for the effects of blocking or turbulence. It is believed that the omission of these corrections does not appreciably affect the derivatives of the forces and moments with respect to yaw angle and wing-tip helix angle (reference 3).

RESULTS AND DISCUSSION

Presentation of Data

The longitudinal characteristics of the various model configurations are shown as curves of α , C_X , and C_m plotted against C_L in figures 6, 7, and 8, respectively. The static lateral-stability parameters C_{l_ψ} , C_{n_ψ} , and C_{Y_ψ} are plotted in figures 9, 10, and 11, respectively; and the rolling derivatives C_{l_p} , C_{n_p} , and C_{Y_p} are presented in figures 12, 13, and 14, respectively. The data for the 10 model configurations are divided into three groups in each figure. The groups are (1) wing with split flaps, (2) wing with slats or nose flap, and (3) wing with combinations of split flaps and slats. The characteristics of the plain wing are included in each of the groups in order to provide a basis for comparison with results obtained with various high-lift devices installed.

Characteristics of Plain Wing

The characteristics of the plain wing generally were good in that there were no abrupt changes in any of the derivatives up to approximately maximum lift. Tests of other swept wings (reference 4) had indicated large changes in the derivatives at moderate lift coefficients. The more favorable characteristics of the present wing probably are a result of the moderate sweep angle in combination with a low aspect ratio.

The pitching-moment curve of figure 8 is essentially linear up to the stall and has a stable break at the stall.

The effective dihedral parameter C_{l_ψ} increased linearly with lift coefficient up to approximately maximum lift (fig. 9) and then decreased very rapidly beyond maximum lift. The directional stability of the

model $C_{n\psi}$ increased approximately as the square of the lift coefficient (fig. 10) as might be expected from the theory of reference 5. At about the maximum lift coefficient, $C_{n\psi}$ broke in a positive direction.

The damping in roll C_{l_p} (fig. 12) showed some increase with lift coefficient and, although this trend is not indicated by theory, it has been observed in other tests of swept wings (references 4 and 6). Negative damping (positive C_{l_p}) was obtained beyond maximum lift, indicating that the model would autorotate if it were free to rotate. The yawing moment due to roll C_{n_p} was negative at all lift coefficients below maximum lift but became positive beyond maximum lift (fig. 13).

Some of the important measured derivatives of the model are summarized in table I. The experimental results are compared with the approximate theory of reference 5 and, where possible, with the theory of Weissinger (references 7 and 8). The comparison between theory and experiment generally is considered to be fair with the exception of C_{n_p}/C_L . The difference between the theoretical and measured values of C_{n_p}/C_L probably is caused by the wing-tip suction forces associated with asymmetric load conditions. Such forces were not accounted for in reference 5. Reference 9 indicates that good agreement between theoretical and measured values of C_{n_p}/C_L might be obtained if the tip suction forces were accounted for.

Effects of Split Flaps

The 0.5-span and 1.0-span split flaps produced lift-coefficient increments of about 0.33 and 0.48, respectively, and these increments remained approximately constant, even to the maximum lift coefficient. Tests of other swept wings (references 1 and 10) have indicated that flap effectiveness in producing lift generally decreases with increase in lift coefficient.

Split flaps increased the longitudinal force very appreciably and made the pitching moment more negative. The slope of the pitching-moment curve was not appreciably affected by the 0.5-span split flaps; however, the 1.0-span flaps made the slope of the pitching-moment curve less negative. The 0.5-span split flaps generally made $C_{l\psi}$ less positive and the 1.0-span split flaps made $C_{l\psi}$ more positive. These displacements of the $C_{l\psi}$ -curve probably were caused by the shift in the center of

pressure of the wing when flaps were deflected. The 0.5-span split flaps shift the center of pressure inboard thus giving the lift forces on the wing panels shorter moment arms and making $C_{l_{\psi}}$ less positive. The 1.0-span split flaps shifted the center of pressure slightly outward (because the flaps did not extend through the fuselage) and made the $C_{l_{\psi}}$ -curve slightly more positive.

The addition of split flaps generally caused minor displacements of the curves of the derivatives $C_{n_{\psi}}$, C_{n_p} , and C_{Y_p} plotted against lift coefficient. The actual mechanism of the flap effect on these derivatives is rather complicated and has not yet been fully analyzed. At low and moderate lift coefficients the derivative C_{l_p} was almost unaffected by the addition of split flaps. In this case the explanation seems to be straightforward, since the addition of split flaps would be expected to have little effect on either the magnitude or the location of the center of pressure of the incremental load caused by rolling. For the model investigated, the addition of split flaps invariably caused an extension to higher lift coefficients of the trends in the derivatives that were noted at low lift coefficients for the plain wing.

Effects of Slats and Nose Flaps

The addition of slats or nose flaps caused the lift curve to be extended to higher angles of attack, thus providing increments in maximum lift coefficient amounting to 0.18 for the 0.5-span slat, 0.39 for the 1.0-span slat, and 0.27 for the 1.0-span nose flap. The nose flap and slats tended to move the aerodynamic center slightly forward, as is indicated by the decreased negative slopes of the pitching-moment curves (fig. 8). A forward shift in aerodynamic center would be expected since the nose flap and slats effectively extend the leading edge of the wing forward.

In general, the leading-edge slats and nose flaps caused very little displacement of the curves for the various stability derivatives at low and moderate lift coefficients. The primary effect appeared to amount to extensions of the linear (or smooth) portions of the curves to higher lift coefficients; however, the nose flap was not as effective as the slats in maintaining the linear trends to higher lift coefficients. A relatively large displacement, in a negative direction, of the $C_{l_{\psi}}$ -curve resulted from the addition of the 1.0-span slat. The slats and nose flaps caused small increases in the damping in roll (negative C_{l_p}) at moderate lift coefficients. This probably results from the effective increase in wing area that accompanied the addition of either the nose flaps or slats.

Effects of Combinations of Split Flaps and Slats

In general, combinations of split flaps and slats had two major effects on the wing characteristics. One of these effects was the extension of the linear portion of the curves of wing characteristics to higher lift coefficients, and the other effect was the displacements of some of the curves. The data of figures 6 to 14 indicate that these extensions and displacements are approximately what would be expected from the results obtained for the effects of split flaps alone and slats alone. Figure 6 indicates that the combination of the wing with 1.0-span slats and 0.5-span split flaps produces very nearly the same maximum lift coefficient as the wing with 1.0-span slats and 1.0-span split flaps; however, the pitching-moment variation at the stall is not as satisfactory for the former combination as for the latter combination. An effect shown by the combination of split flaps and slats (not shown by slats alone or split flaps alone) is the change in lift-curve slope at low lift coefficients for some of the configurations (fig. 6). It is believed that the increase in damping in roll at low lift coefficients of some of the configurations (fig. 12) is associated with the changes in the lift-curve slope.

CONCLUSIONS

The results of tests made to determine the effects of high-lift devices on the stability parameters of a tapered 37.5° sweptback wing of aspect ratio 3 in straight and rolling flow have led to the following conclusions:

1. The variation of the parameters with lift coefficient is essentially the same, at low and moderate lift coefficients, for all the configurations tested.
2. The high-lift devices extended the initial trend of the parameters to higher lift coefficients and in some cases caused small displacements of the curves plotted against lift coefficient.
3. Nose flaps were not as effective as slats in extending the initial trend of the curves to high lift coefficients.
4. Combinations of split flaps and slats produced effects which were approximately equal to the sum of the effects of split flaps alone and slats alone.

Langley Aeronautical Laboratory
National Advisory Committee for Aeronautics
Langley Field, Va.

REFERENCES

1. Lichtenstein, Jacob H.: Effect of High-Lift Devices on the Low-Speed Static Lateral Stability and Yawing Characteristics of an Untapered 45° Sweptback Wing. NACA RM No. L8G20, 1948.
2. MacLachlan, Robert, and Letko, William: Correlation of Two Experimental Methods of Determining the Rolling Characteristics of Unswept Wings. NACA TN No. 1309, 1947.
3. Bird, John D., Lichtenstein, Jacob H., and Jaquet, Byron M.: Investigation of the Influence of Fuselage and Tail Surfaces on Low-Speed Static Stability and Rolling Characteristics of a Swept-Wing Model. NACA RM No. L7H15, 1947.
4. Feigenbaum, David, and Goodman, Alex: Preliminary Investigation at Low Speeds of Swept Wings in Rolling Flow. NACA RM No. L7E09, 1947.
5. Toll, Thomas A., and Queijo, M. J.: Approximate Relations and Charts for Low-Speed Stability Derivatives of Swept Wings. NACA TN No. 1581, 1948.
6. Hunton, Lynn W., and Dew, Joseph K.: Measurements of the Damping in Roll of Large-Scale Swept-Forward and Swept-Back Wings. NACA RM No. A7D11, 1947.
7. DeYoung, John: Theoretical Additional Span Loading Characteristics of Wings with Arbitrary Sweep, Aspect Ratio, and Taper Ratio. NACA TN No. 1491, 1947.
8. Van Dorn, Nicholas H., and DeYoung, John: A Comparison of Three Theoretical Methods of Calculating Span Load Distribution on Swept Wings. NACA TN No. 1476, 1947.
9. Brewer, Jack D., and Fisher, Lewis R.: Effect of Taper Ratio on the Low-Speed Rolling Stability Derivatives of Swept and Unswept Wings of Aspect Ratio 2.61. NACA RM No. L8H18, 1948.
10. Salmi, Reino J., and Fitzpatrick, James E.: Yaw Characteristics and Sidewash Angles of a 42° Sweptback Circular-Arc Wing with a Fuselage and with Leading-Edge and Split Flaps at a Reynolds Number of 5,300,000. NACA RM No. L7I30, 1947.

TABLE I

COMPARISON OF MEASURED AND CALCULATED PARAMETERS FOR THE PLAIN WING

Parameters	Experimental	Calculated (reference 5)	Calculated (references 7 and 8)
$C_{L\alpha}$	0.053	0.047	0.048
$C_{L\psi}/C_L$.0047	.0035	-----
$C_{n\psi}/C_L^2$	-.0012	-.0010	-----
C_{Lp}	-.250	-.230	-.237
C_{np}/C_L	-.090	-.047	-----
C_{Yp}/C_L	.45	.47	-----

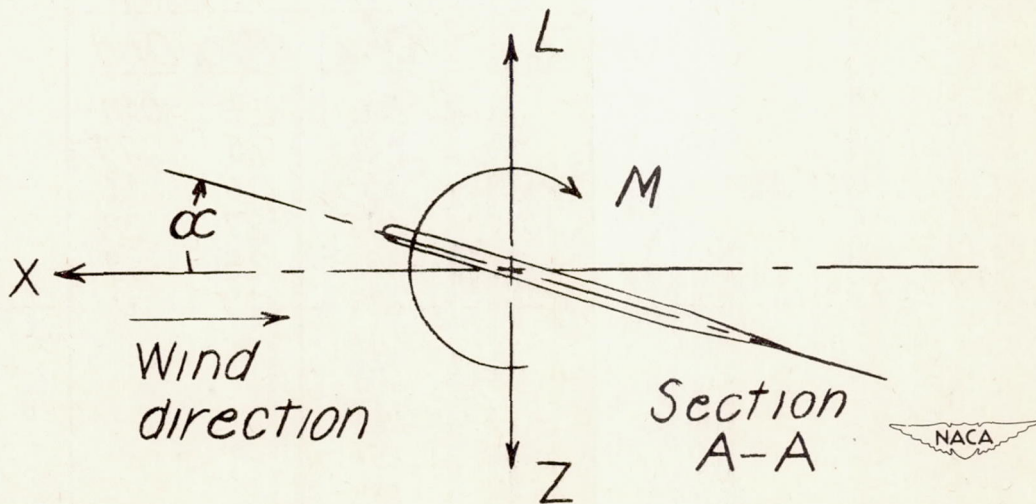
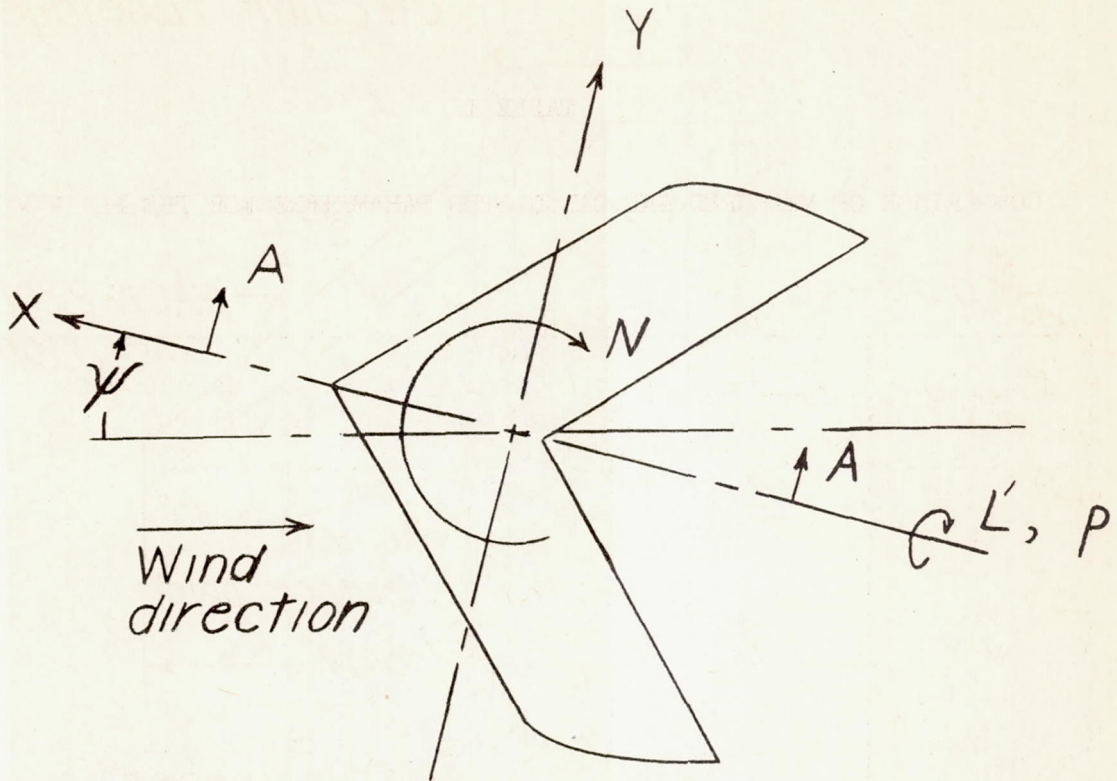
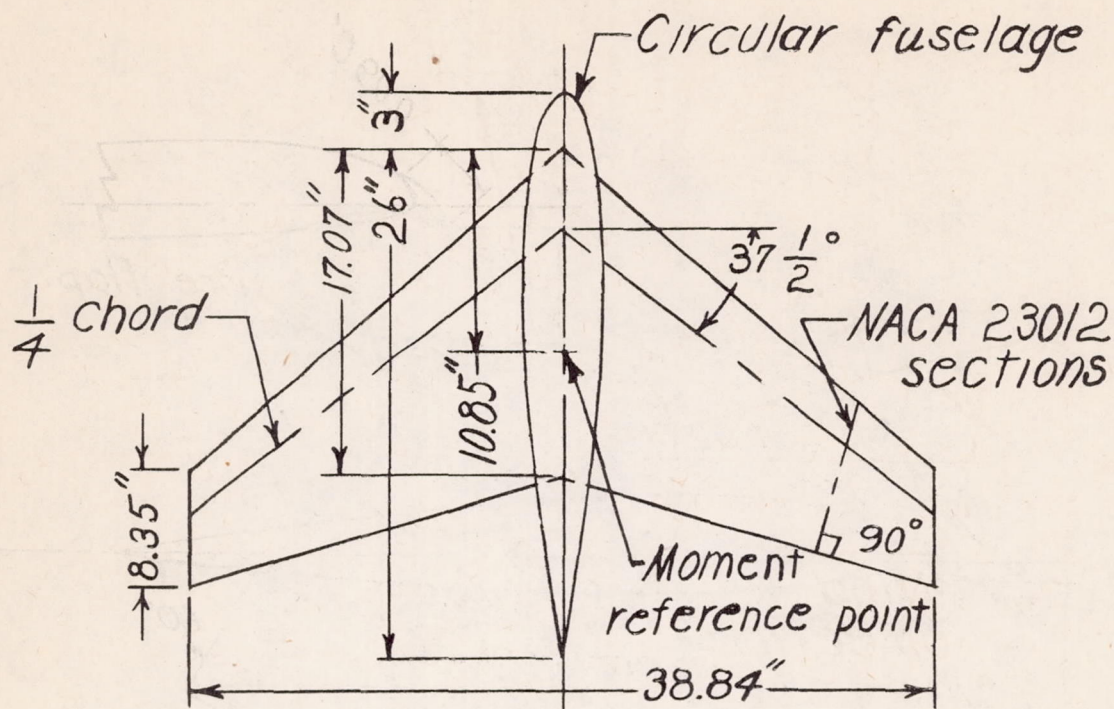


Figure 1.- System of stability axes. Arrows indicate positive directions of forces, moments, and displacements.



Fuselage coordinates, inches

Nose radius 0.78					
<u>Sta.</u>	<u>Ord.</u>	<u>Sta.</u>	<u>Ord.</u>	<u>Sta.</u>	<u>Ord.</u>
0.50	0.75	11.00	2.00	24	0.91
1.00	.98	12	2.00	25	.74
1.50	1.16	13	1.99	26	.56
2.00	1.30	14	1.97	27	.38
2.50	1.41	15	1.93	28	.19
3.00	1.50	16	1.88	29	0
4	1.65	17	1.81		
5	1.75	18	1.73		
6	1.83	19	1.63		
7	1.89	20	1.51		
8	1.94	21	1.38		
9	1.98	22	1.25		
10	1.99	23	1.09		

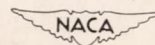


Figure 2.- Drawing of wing-fuselage combination.

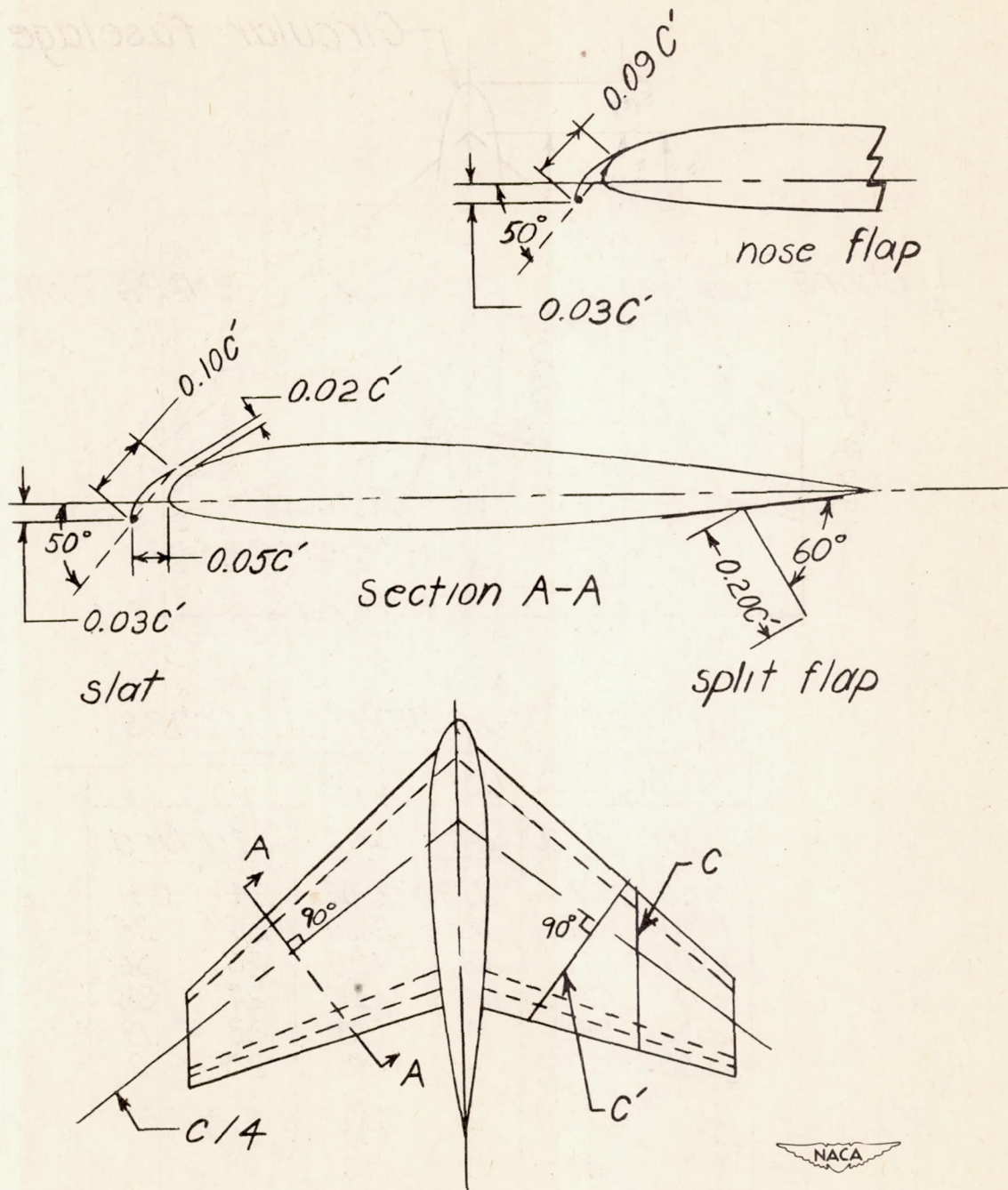
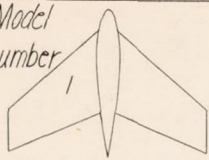
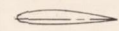
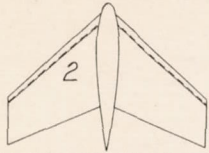
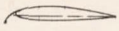
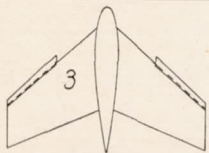
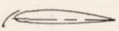
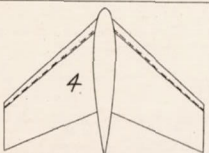
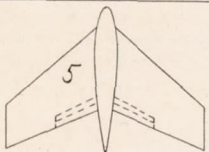
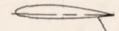
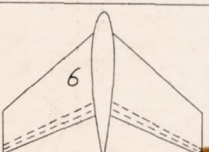
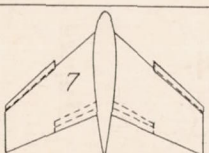
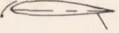
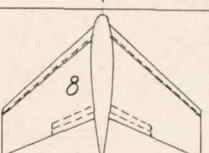
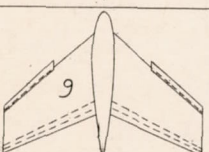
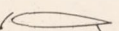
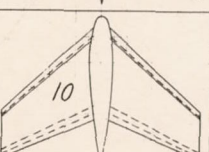


Figure 3.- Details of split flaps and slats.

Configurations tested		Typical section
Model number 1		
2		
3		
4		
5		
6		
7		
8		
9		
10		

Model number	Model designation
1	Wing
2	Wing with 1.0b nose flaps
3	Wing with 0.5b slats
4	Wing with 1.0b slats
5	Wing with 0.5b split flaps
6	Wing with 1.0b split flaps
7	Wing with 0.5b slats and 0.5b split flaps
8	Wing with 1.0b slats and 0.5b split flaps
9	Wing with 0.5b slats and 1.0b split flaps
10	Wing with 1.0b slats and 1.0b split flaps

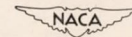
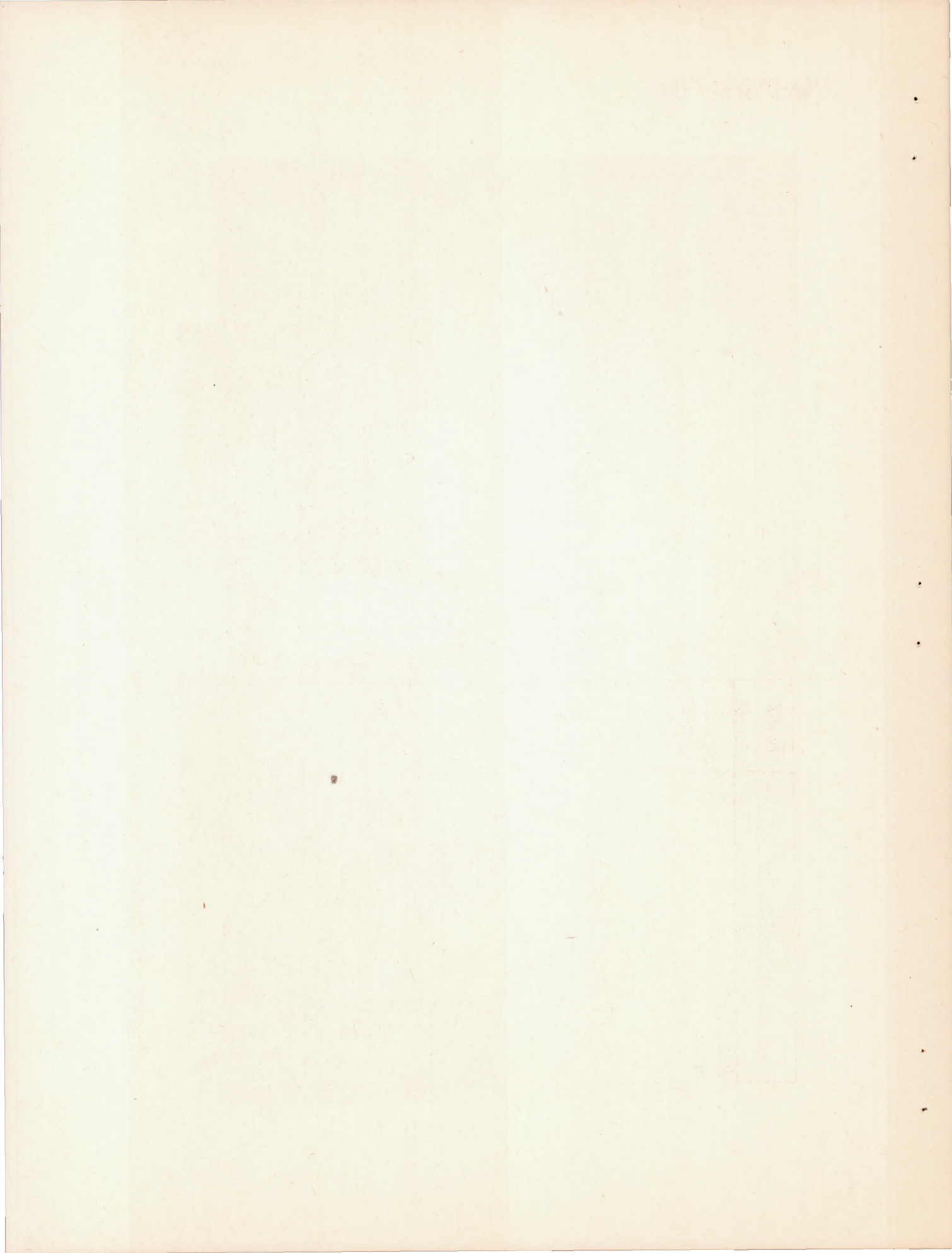


Figure 4.- Model configurations tested.



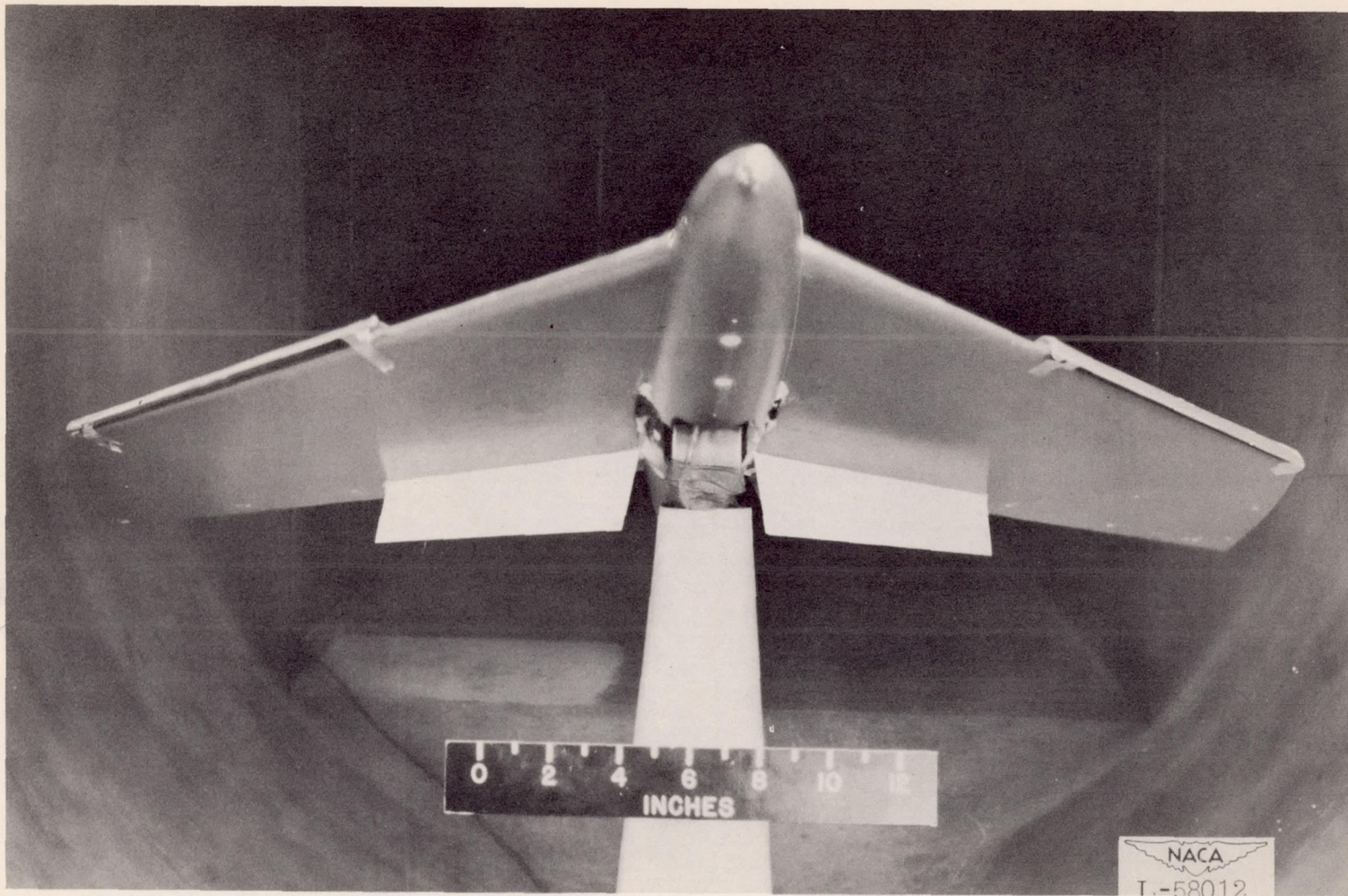
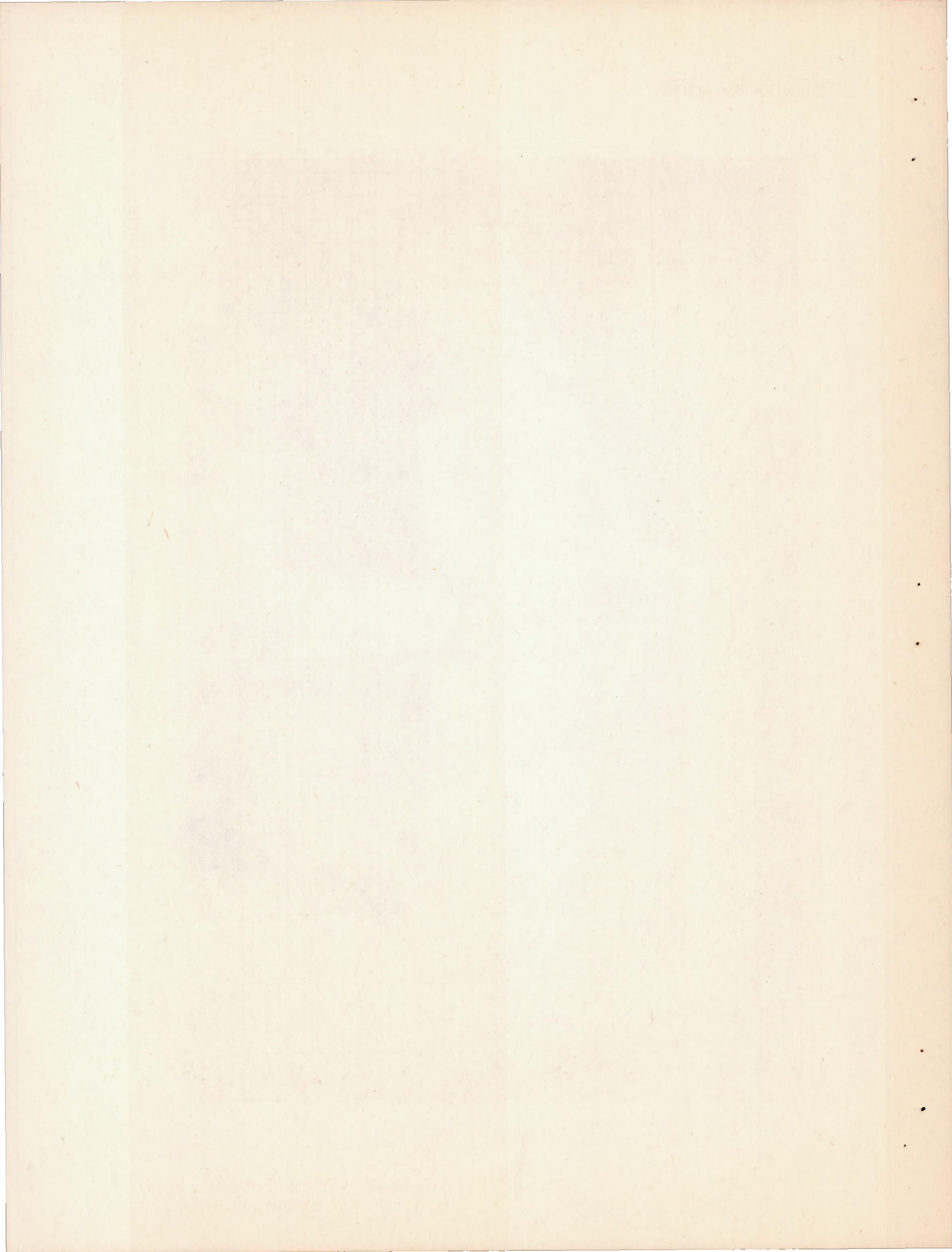


Figure 5.- Photograph of model in tunnel. Model has 0.5-span split flaps and 0.5-span slats.



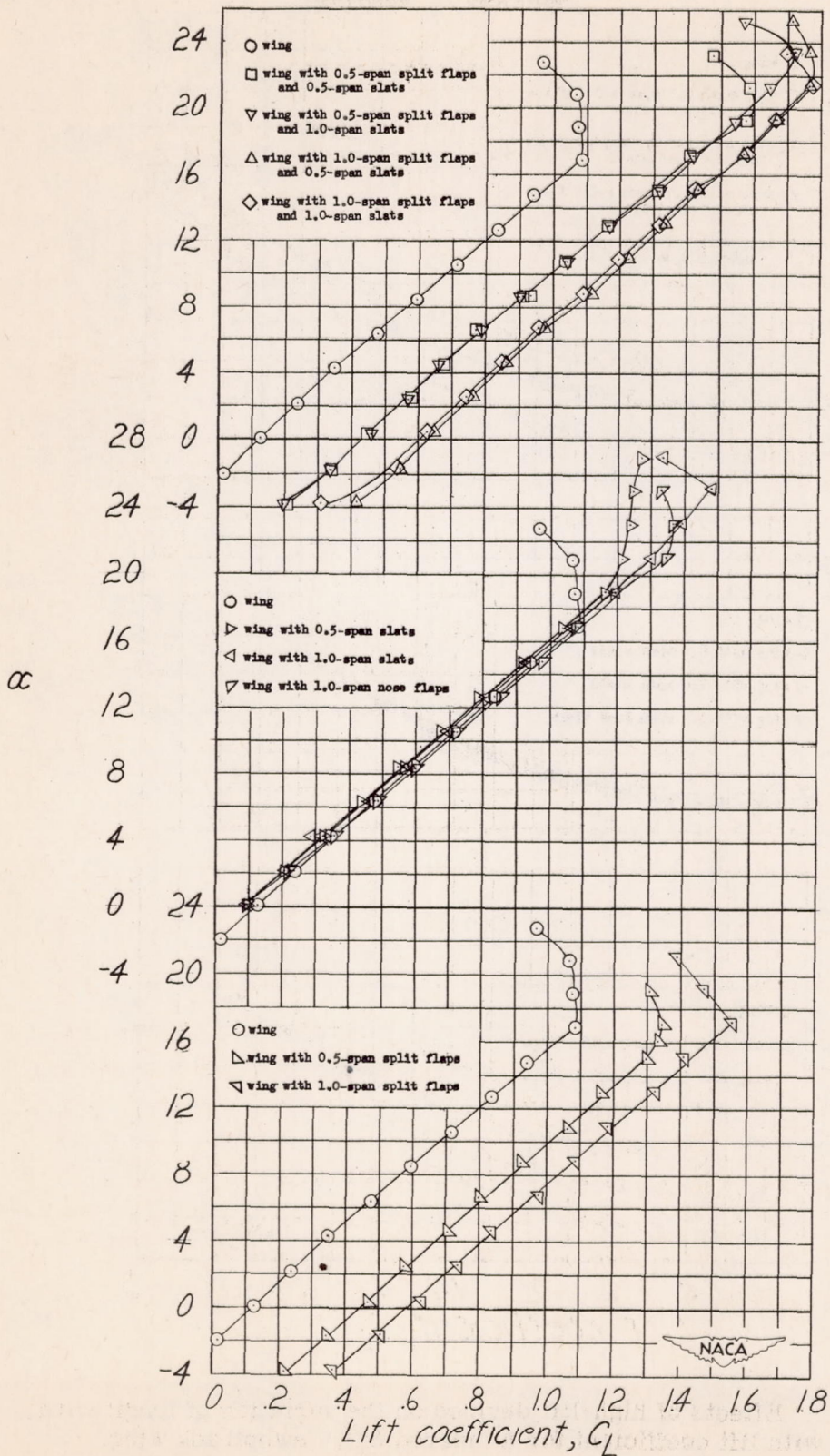


Figure 6.- Effects of high-lift devices on the variation of angle of attack with lift coefficient for a tapered 37.5° sweptback wing.

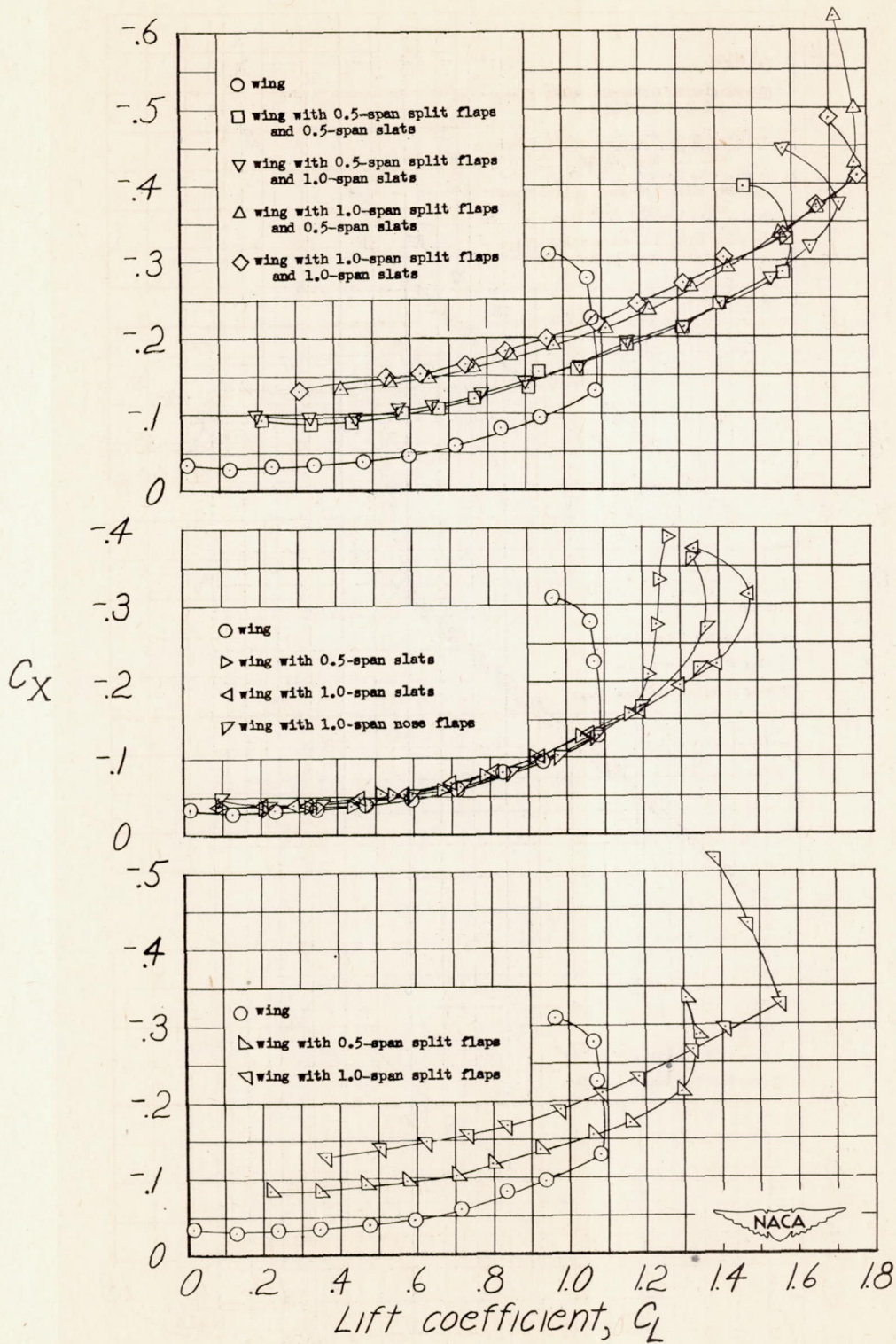


Figure 7.- Effects of high-lift devices on the variation of longitudinal force with lift coefficient for a tapered 37.5° sweptback wing.

C_m

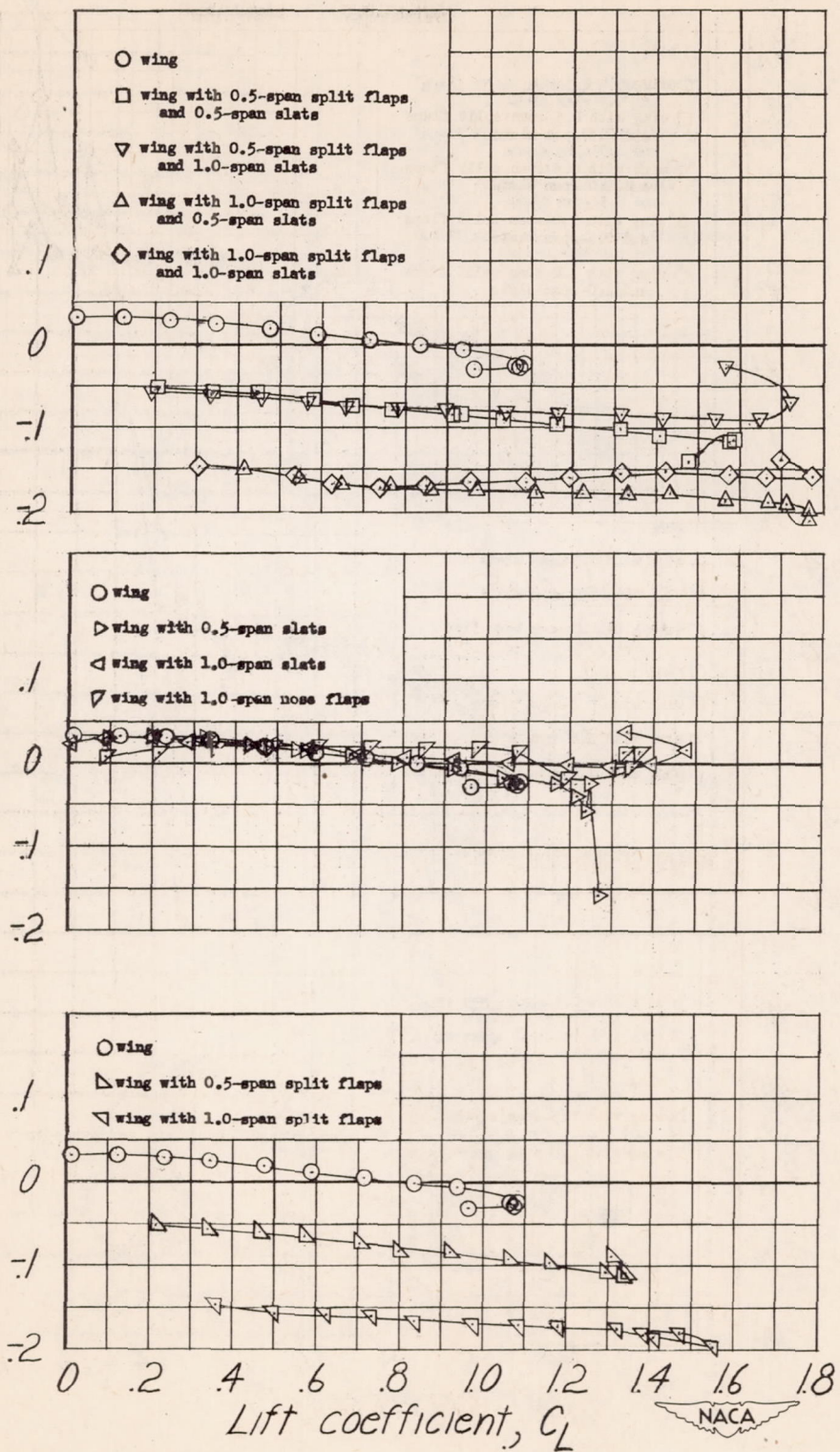


Figure 8.- Effects of high-lift devices on the variation of pitching moment with lift coefficient for a tapered 37.5° sweptback wing.

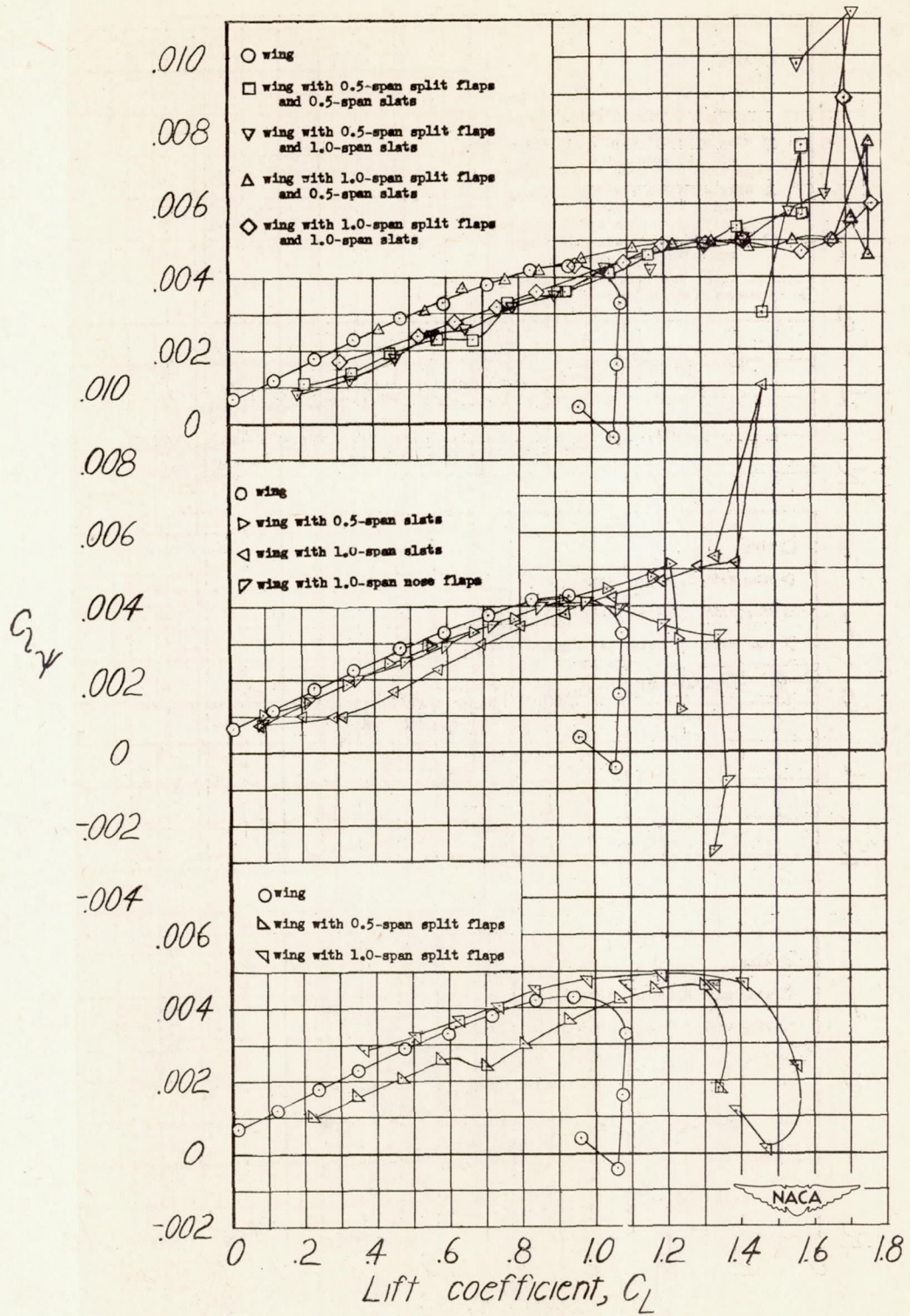


Figure 9.- Effects of high-lift devices on the variation of $C_{L\alpha}$ with lift coefficient for a tapered 37.5° sweptback wing.

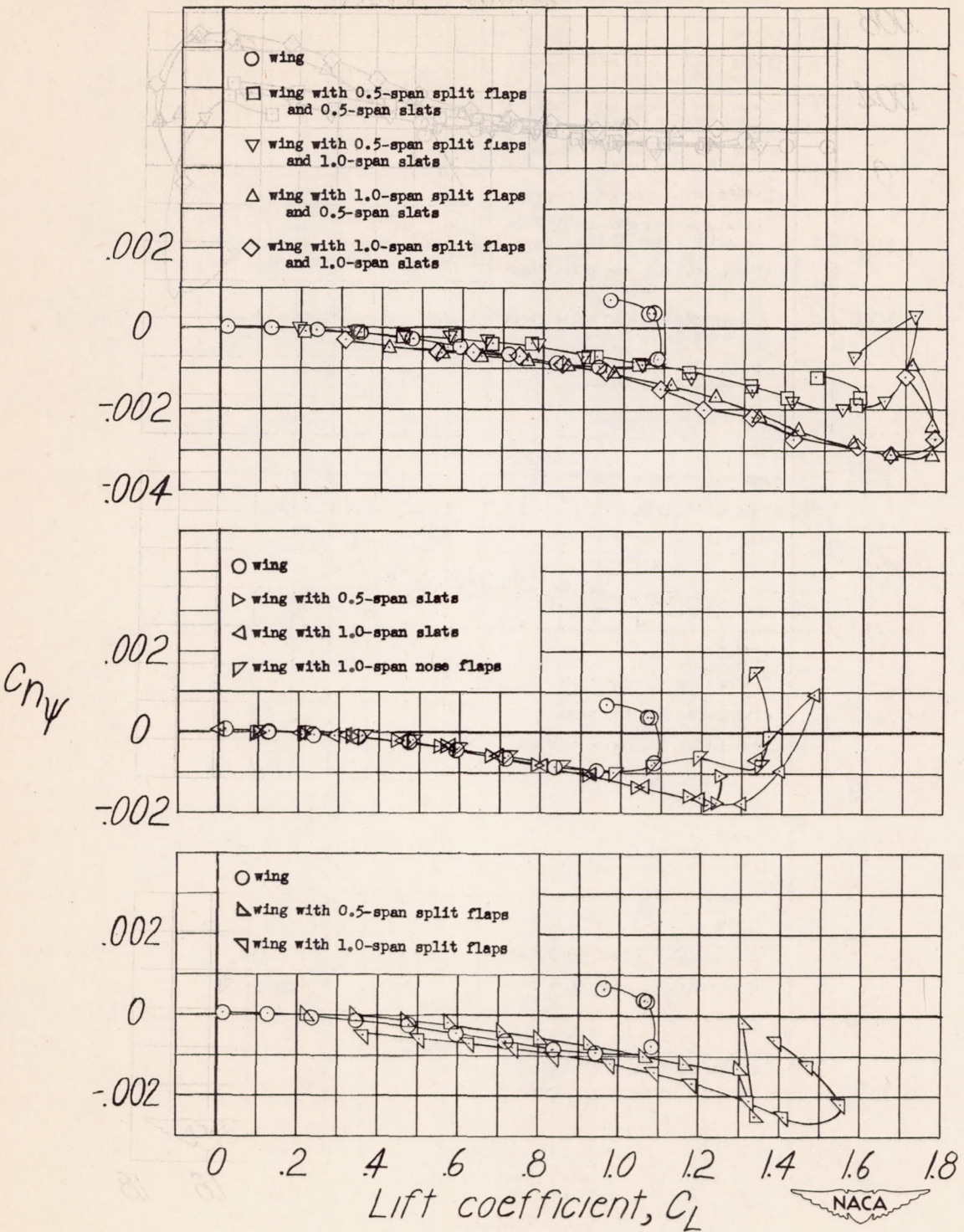


Figure 10.- Effects of high-lift devices on the variation of $C_{n\psi}$ with lift coefficient for a tapered 37.5° sweptback wing.

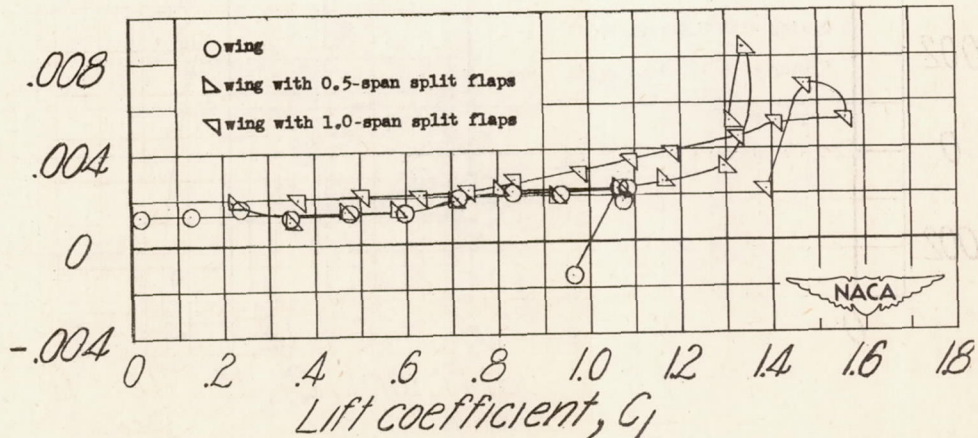
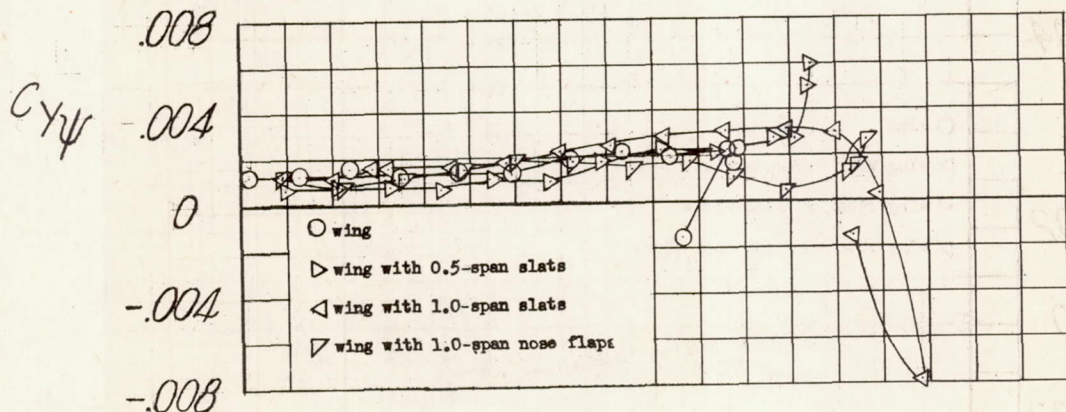
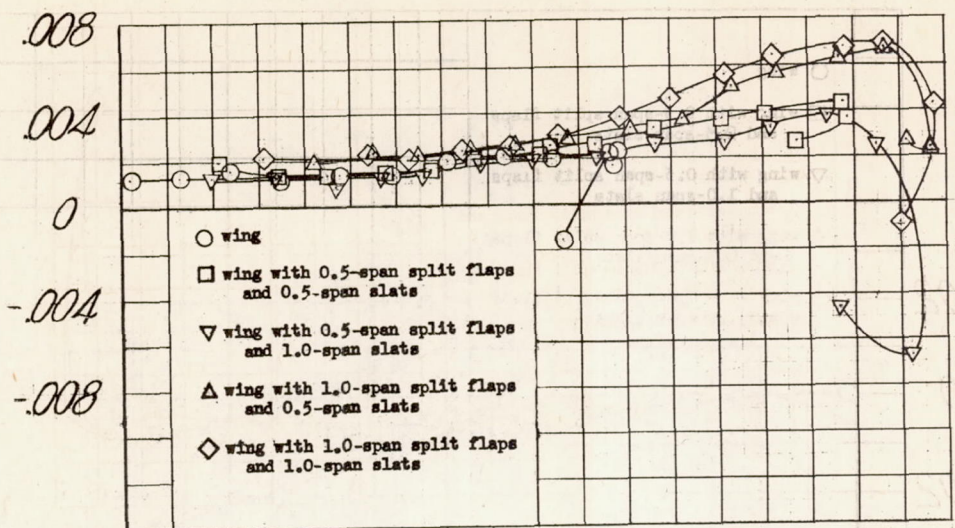


Figure 11.- Effects of high-lift devices on the variation of $C_{Y\psi}$ with lift coefficient for a tapered 37.5° sweptback wing.

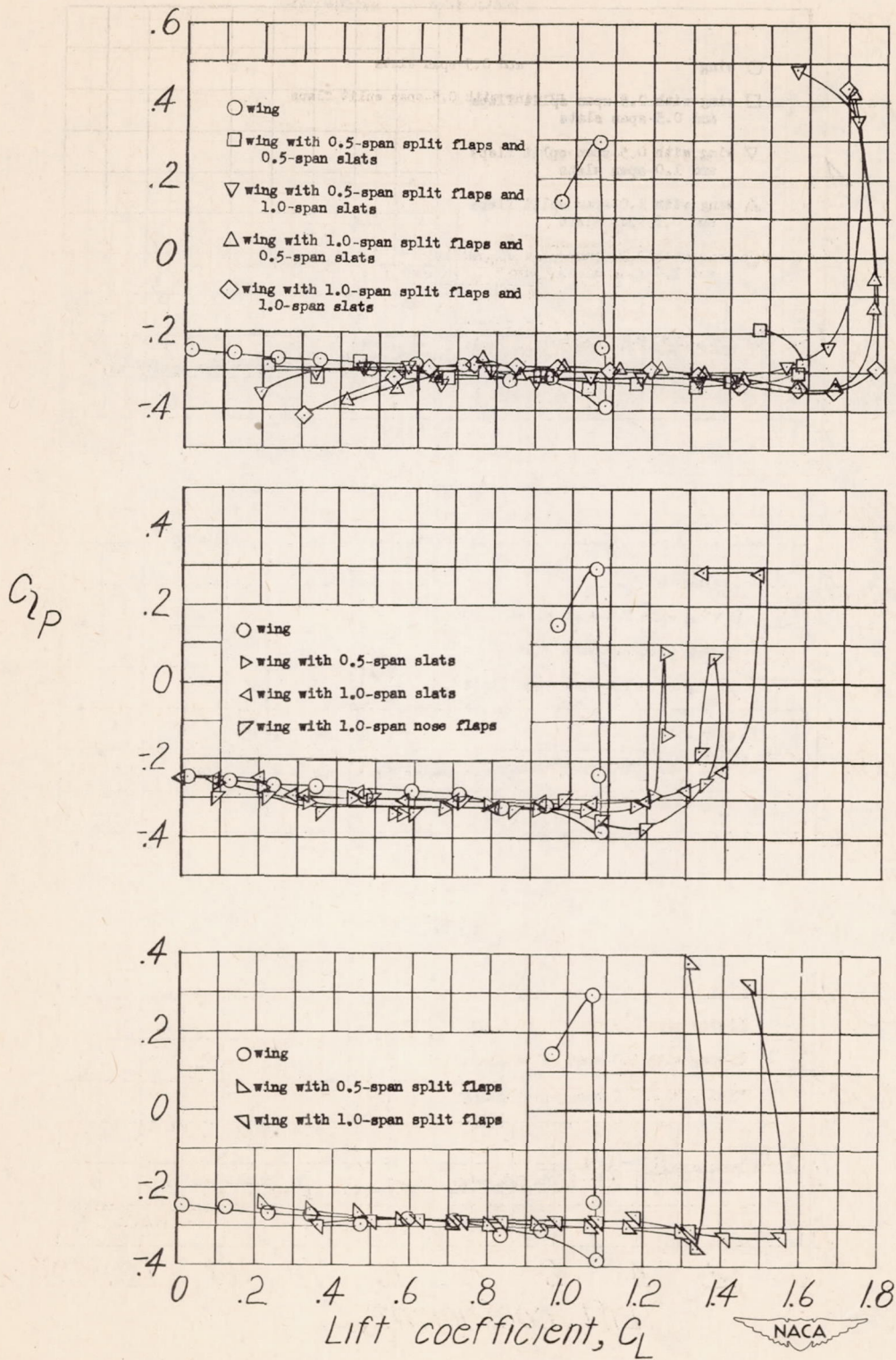
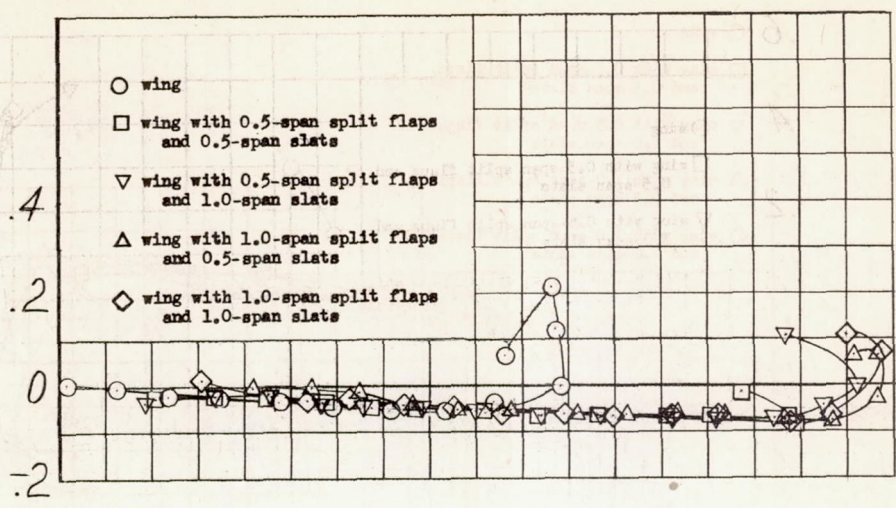


Figure 12.- Effects of high-lift devices on the variation of C_{z_p} with lift coefficient for a tapered 37.5° sweptback wing.



C_{np}

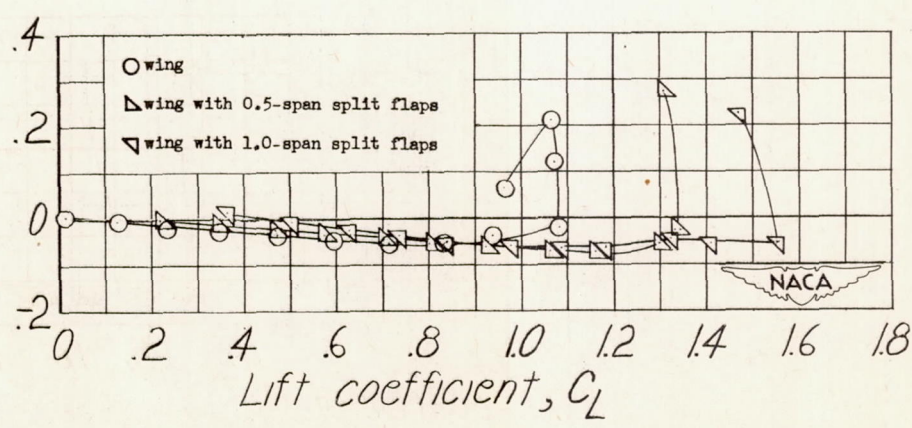
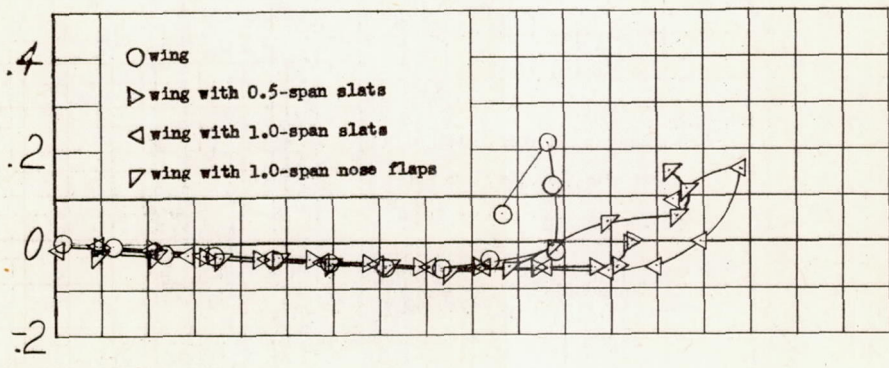


Figure 13.- Effects of high-lift devices on the variation of C_{np} with lift coefficient for a tapered 37.5° sweptback wing.

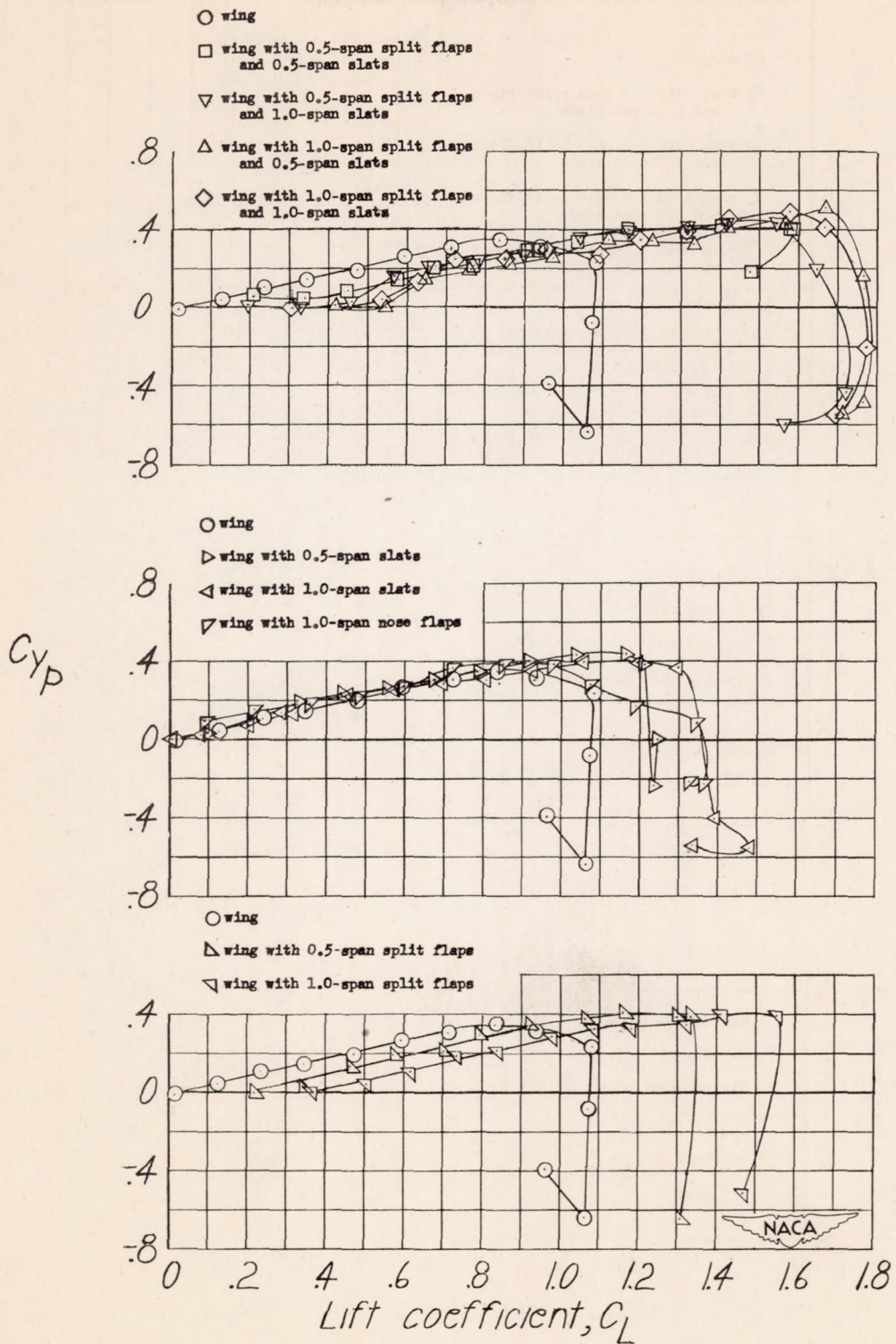


Figure 14.- Effects of high-lift devices on the variation of C_{Yp} with lift coefficient for a tapered 37.5° sweptback wing.